The cone energy is independent of the moduli G and thus independent of the elastic thickness h (*23*). The cone energy remains a significant fraction of the tetrahedron energy for all tetrahedra studied. Nevertheless, the asymptotic scaling gives less than 10% error for tetrahedra larger than about 10^3 times their thickness (for example, a 10-cm tetrahedron made of standard 0.1-mm-thick office paper). The simulated sheets of Tersoff (*24*) and of Kroll (*22*) did not approach these size-to-thickness ratios; thus, it is not surprising that they saw no evidence for the energy scaling predicted here.

The ridges suggest an approach for describing a strongly crumpled sheet. From common observation, crumpled sheets contain a large number of vertices. We may suppose that pairs of adjacent vertices give rise to ridges like the ones seen in our simple shapes. The neighboring ridges can be expected to influence one another. Still, this mutual influence cannot be too great. Our study has shown that well-developed ridges are but little influenced by the surface at distances of order X from the ridge line. This is natural, because the ridge energy is concentrated at distances much smaller than X from this line. We are led to treat the ridges as independent, at least as a first approximation. Thus, we may find the approximate energy of a given crumpled sheet from its ridge lengths X_i by simply adding the individual energies to obtain a total energy $E \approx \kappa \Sigma_i (X_i/h)^{1/3}$.

We expect the stretching-ridge concept to contribute to future understanding of the crumpled materials like those in Fig. 1. When the ridges are a few hundred times longer than the membrane thickness, they give a quantitative account of the deformation energy. The ridge concept should aid in the design of macroscopic energy-absorbing materials such as packing material (*4*) and protective vehicle structures (*3*), for example, by placing defects to control where ridges form. Knowledge about ridges may aid the understanding of microscopic phenomena such as the collapse of graphite membranes (*6*) and the passage of blood cells through capillaries (*25*), and it may elucidate large-scale phenomena such as the buckling of the Earth's crust (*26*).

REFERENCES AND NOTES

1. *Post-Buckling of Elastic Structures*, proceedings of the *Euromech Colloquium*, no. 200, Matrafured, Hungary, 5 to 7 October 1985 (Elsevier, Amsterdam, 1986).
2. N. Yamaki, *Elastic Stability of Circular Cylindrical Shells* (North-Holland, New York, 1984).
3. P. Stutenkemper and R. Brasche, in *International Technical Conference on Experimental Safety Vehicles*, sponsored by the Government of France, Paris, 5 to 8 June 1979 (Government Printing Office, Washington, DC, 1980), pp. 321–329.
4. C. E. Crede, in *Symposium on Simulated Service Testing of Packaging*, Sponsored by the Administrative Committee on Simulated Service Testing, New York, NY, 1962 (American Society for Testing and Materials, Philadelphia, PA, 1963), pp. 1–49.
5. R. E. Newton, in *Shock and Vibration Handbook*, C. M. Harris and C. E. Crede, Eds. (McGraw-Hill, New York, 1988), p. 31-1; P. E. Franklin and M. T. Hatae, *ibid.*, p. 41-1.
6. M. S. Spector, E. Naranjo, S. Chiruvolu, J. A. Zasadzinski, *Phys. Rev. Lett.* **73**, 2867 (1994).
7. E. Sackmann *et al.*, *Ber. Bunsen-ges. Phys. Chem.* **89**, 1198 (1985).
8. J. B. C. García, M. A. F. Gomes, T. I. Jyh, T. I. Ren, *J. Phys. A. Gen. Phys.* **25**, L353 (1992).
9. F. Abraham, paper presented at the Workshop on Biomaterials, University of California, Santa Barbara, CA, 31 August 1994.
10. Y. Kantor, M. Kardar, D. R. Nelson, *Phys. Rev. Lett.* **57**, 791 (1986).
11. R. Scheidl and H. Troger, in (*1*), p. 293.
12. M. Ortiz and G. Giola, *J. Mech. Phys. Solids* **41**, 531 (1994).
13. H. S. Seung and D. R. Nelson, *Phys. Rev. A* **38**, 1005 (1988).
14. D. Nelson, T. Piran, S. Weinberg, Eds., *Statistical Mechanics of Membranes and Surfaces* (World Scientific, Singapore, 1989).
15. D. R. Nelson and L. Peliti, *J. Phys. (Paris)* **48**, 1085 (1987); F. David and E. Guitter, *Europhys. Lett.* **5**, 709 (1988).
16. L. D. Landau and E. M. Lifshitz, *Theory of Elasticity* (Pergamon, Oxford, 1986), sections 14 and 15. Our cylindrical bending modulus κ is denoted there as D.
17. See, for example, G. Gerard, *Handbook of Structural Stability* (New York University, New York, NY, 1956).
18. In (*14*), p. 143.
19. T. A. Witten and H. Li, *Europhys. Lett.* **23**, 51 (1993).
20. A full description requires two stretching and two bending moduli; however, these details are not important for our scaling argument.
21. D. C. Morse and T. C. Lubensky, *J. Phys. II* **3**, 531 (1993).
22. Z. Zhang, H. T. Davis, D. M. Kroll, *Z. Phys. B* **97**, 337 (1995).
23. More precisely, the cone energy is independent of h in the limit that h is much smaller than the lattice spacing a. In our numerical studies h varied from a to a few percent of a. Accordingly, we observed a few-percent dependence of the cone energy on h.
24. J. Tersoff, *Phys. Rev. B* **46**, 15546 (1992).
25. W. H. Reinhart *et al.*, *Biorheology* **28**, 537 (1991).
26. See, for example, R. J. Chorley, S. A. Schumm, D. E. Sugden, *Geomorphology* (Methuen, London, 1984), chap. 7.
27. Y. L. Kergosien, H. Gotoda, T. L. Kunii, *IEEE Comput. Graphics Appl.* **14**, 40 (1994).
28. R. R. Chianelli, E. B. Prestridge, T. A. Pecoraro, J. P. DeNeufville, *Science* **203**, 1105 (1979).

29. We are grateful to J. Gao, N. Lebovitz, S. Antman, and S. Nagel for assistance and discussions. Supported by NSF under award number DMR-9205827 and through its Materials Research Science and Engineering Center Program under award number DMR-9400379. S.G. was supported as a summer intern by the NSF Research Experiences for Undergraduate Program under NSF Research Experience for Undergraduates site grant Phy-9212351. We thank the authors of (*27*) for providing the image for Fig. 1A.

3 July 1995; accepted 29 September 1995

Autoencapsulation Through Intermolecular Forces: A Synthetic Self-Assembling Spherical Complex

Robert S. Meissner, Julius Rebek Jr.,* Javier de Mendoza

The synthesis and characterization of a system for the study of molecular recognition phenomena are described. The system involves a tetraurea molecule that is capable of assembly into various associated states through hydrogen bonding. In organic solvents, the dynamic transition between a low-ordered (aggregate) state and a highly ordered dimeric assembly can be induced by the introduction of smaller molecules of appropriate size and shape. These smaller molecules, such as benzene, adamantanes, and ferrocenes, act as guests that occupy the pseudospherical capsule formed by the dimeric host. Among various guests, those that best fill the cavity and offer chemical complementarity to the host are preferentially encapsulated.

How molecules fit together—molecular recognition—can be explored with biological macromolecules and with synthetic structures of low molecular weight. Recognition expresses structural information and takes the form of complementarity in size, shape, and chemical surfaces. A subtle expression of information is possible with self-complementary molecules. Multiple copies of such molecules can give rise to ordered superstructures—assemblies—with functions that are unique to their assembled states. In molecular assembly formation, favorable binding forces (enthalpy) compete with energy loss due to the decreased freedom of the individual subunits (entropy). Guest molecules that match a host assembly in size and shape interact to produce an increased van der Waals attraction, and those guests with functional groups capable of forming hydrogen bonds with the host produce increased electrostatic attraction. Guests that maximize the attractive forces are preferred (*1*). Here we describe a molecule that assembles to provide a host for the reversible encapsulation of sizable, complementary guests (*2*).

Molecule **1** consists of 13 fused rings that

R. S. Meissner and J. Rebek Jr., Massachusetts Institute of Technology, Department of Chemistry, Cambridge, MA 02139, USA.
J. de Mendoza, Universidad Autonoma de Madrid, Departamento de Quimica, Cantoblanco, 28049 Madrid, Spain.

*To whom correspondence should be addressed.

give it an extended, rigid structure (Fig. 1A). The stereoisomer shown presents the R groups on the same face of the molecule as the central ethylene bridge. This feature permits the structure to assume low-energy conformations of an overall C-shape, with all R groups positioned on its convex surface. As in other cases of molecular assembly formation (*3*), hydrogen bonds provide the attractive forces. The hydrogen bond acceptors on the ends of the structure (the four N–H bonds) are complementary to the hydrogen bond donors near its center (the four carbonyl oxygens). When two molecules of **1** come together with their concave surfaces opposed, a structure of roughly spherical shape can result. The assembly is modeled (*4*) in Fig. 1B, where the hydrogen bonding sites and the gentle curvature of the units are highlighted.

In the synthesis of compound **1a** (Fig. 2), we took advantage of its symmetry and modular nature. The urea-containing termini of the target were made by sequential treatment of tetrabromodurene (**2**) with *tert*-butyl hydrazodiformate (**3**) and diphenylglycoluril (**5**). Although only modest yields of **6** were obtained, this procedure avoids the use of protecting groups at the remaining reactive sites of **2** and **5** (*5*). Compound **6** was then deprotected with acid to produce the hydrazine salt **7**. The central unit **8** was prepared by a multiple-step process that relied on the Diels-Alder cylcloaddition of the acetylene **9** and the diene **10** as the key reaction (Fig. 3) (*6*). The final assembly fused the tetraacid-chloride **8** to two molecules of hydrazine **7** (Fig. 2). The reaction produced a mixture of the three possible stereoisomers. Isolation of the desired C-shaped isomer was achieved by a combination of extraction and silica gel chromatography. A parallel synthesis, in which each phenyl group was replaced with an isopentyl ester, gave a derivative (**1b**) with greater solubility in organic solvents.

In the solvent benzene-d_6, proton nuclear magnetic resonance (NMR) signals of molecule **1a** are sharp, and downfield shifts were observed for the N–H resonances, characteristic of an ordered, extensively hydrogen-bonded system (Fig. 4A). However, in $CDCl_3$, the molecule dissolved with difficulty and formed a gel-like phase after a few minutes. The spectrum showed broad unresolved peaks (Fig. 4B), and the suspension in the NMR tube could be turned upside down without loss of its contents. Evidently, in this solvent an aggregate of relatively low order was formed.

The more soluble derivative **1b** showed

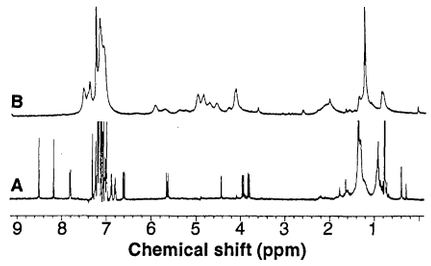

Fig. 4. ^{1}H NMR spectra of **1a**. (**A**) Benzene-d_6 solvent. The signals between 7.2 and 7.0 ppm, and between 2.2 and 0 ppm, are from the solvent and its impurities. (**B**) Chloroform-*d* solvent. The single peak at 7.26 ppm is from the solvent.

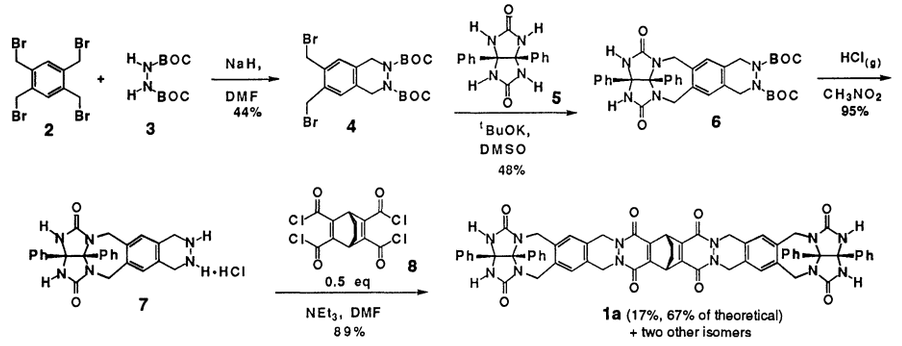

Fig. 2. Synthesis of monomer **1a**. Abbreviations: BOC, *tert*-butoxycarbonyl; DMF, *N,N*-dimethyl formamide; ^{t}BuOK, potassium *tert*-butoxide; Ph, phenyl; DMSO, dimethyl sulfoxide; Net_3, triethyl amine; and eq, equivalents.

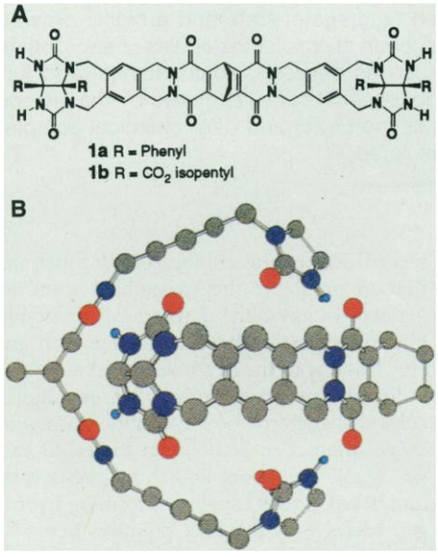

Fig. 1. (**A**) Structural depiction of monomer **1**. (**B**) Energy-minimized (*4*) dimeric depiction of the self-assembled structure **1**. The R groups and some hydrogens have been omitted for clarity. Carbon atoms are gray, nitrogen are dark blue, oxygen are red, and hydrogen are light blue.

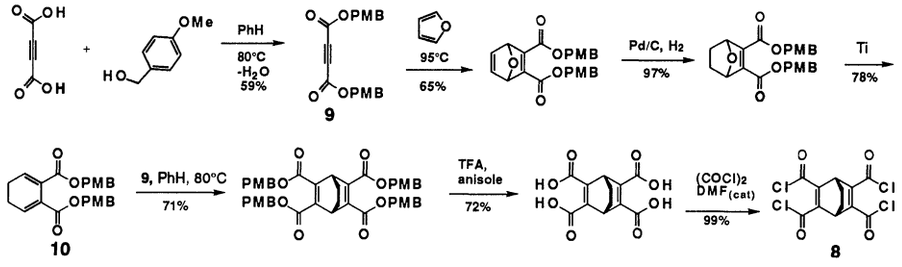

Fig. 3. Synthesis of the central tetraacylchloride. Abbreviations: Me, methyl; PMB, *para*-methoxy benzyl; and TFA, triflouroacetic acid.

Table 1. Stoichiometric and kinetic data. Abbreviations: $[\mathbf{1b}]_{tot}$, total concentration of **1b**; $[guest]_{tot}$, total guest concentration; K_a(app), apparent association constants; and M, molar.

Guest	Stoichiometry*	$[\mathbf{1b}]_{tot}$ (mM)	$[guest]_{tot}$ (mM)	K_a(app) (M^{-1})†
1,3,5,7-tetramethyladamantane	0.9	8.15	40.8	6.7
1-adamantaneamine	1.0	6.70	3.35	190
1-adamantanecarboxamide	0.9	6.70	2.65	310
1-adamantanecarboxylic acid	1.0	6.70	2.65	780
1,3-adamantanedicarboxlic acid	1.0	6.70	−‡	−‡
1-ferrocenecarboxylic acid	1.1	6.40	3.20	280

*Equivalents of guest per equivalent host dimer (±10%). †Calculated with Eq. 1 (*10*). ‡Value was not calculated because of the insolubility of the free guest.

a spectrum similar to that of **1a** in benzene-d_6, but in *para*-xylene-d_{10} it produced broad signals in the NMR spectrum (Fig. 5A). Addition of 1-adamantanecarboxylic acid to the xylene solution led to a significant sharpening of the signals, and a set of upfield signals emerged between −0.1 and −1.0 parts per million (ppm) (Fig. 5B). These can be attributed to an inclusion complex in which two molecules of **1b** surround the 1-adamantanecarboxylic acid; the four benzene rings of the host provide the anisotropic environment that leads to the shielding of the NMR signals of the guest. Similarly, 1,3-adamantanedicarboxylic acid (Fig. 5C), 1-adamantanecarboxamide (Fig. 5D), 1-ferrocenecarboxylic acid (Fig. 5E), 1,3,5,7-tetramethyladamantane (Fig. 5F), 1-adamantaneamine, and ferrocene can also be encapsulated by the dimeric host. In the case of 1,3-adamantanedicarboxylic acid, the guest alone was completely insoluble in the *para*-xylene-d_{10} solvent but was rapidly drawn into solution by encapsulation (*7*).

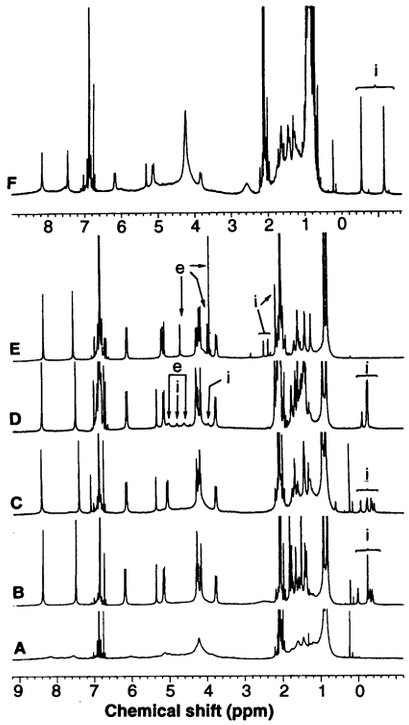

Fig. 5. ^{1}H NMR spectra of **1b** in *para*-xylene-d_{10} solvent with various guests. The signals of the included guest are labeled with an "i," and the excluded guest signals, when resolved, are labeled with an "e." (**A**) Compound **1b** (6.70 mM) in *para*-xylene-d_{10} solvent. The signals between 7.0 and 6.6 ppm, 2.2 and 1.8 ppm, and at 0.17 ppm are from the solvent and its impurities; the residual water signal is at 0.22 ppm. (**B**) Compound **1b** (6.70 mM) in *para*-xylene-d_{10} solvent with 2 equivalents of 1-adamantanecarboxylic acid added. (**C**) Compound **1b** (6.70 mM) in *para*-xylene-d_{10} solvent with 2 equivalents of 1,3-adamantanedicarboxylic acid added. (**D**) Compound **1b** (6.70 mM) in *para*-xylene-d_{10} solvent with 2 equivalents of 1-adamantanecarboxamide added. The labeled guest peaks between 3.6 and 5.0 ppm are the amide N–H signals. (**E**) Compound **1b** (6.40 mM) in *para*-xylene-d_{10} solvent with 2 equivalents of 1-ferrocenecarboxylic acid added. (**F**) Compound **1b** (8.15 mM) in *para*-xylene-d_{10} solvent with 10 equivalents of 1,3,5,7-tetramethyladamantane added.

The spectroscopic observations can be interpreted as follows. In the presence of a solvent ill-suited for encapsulation (the small chloroform or the elongated *p*-xylene), intermolecular hydrogen bonding led to low-order aggregation of the monomer. With the addition of a guest of complementary size and shape, such as benzene or 1,3,5,7-tetramethyladamantane, the spherical dimeric form is favored, because attractive van der Waals interactions between host and guest are maximized within the inclusion complex. The equilibrium is further displaced toward the dimeric capsule when guests such as the functionalized adamantane derivatives or 1-ferrocenecarboxylic acid fill the space and provide hydrogen bonds to the interior surface of the host (Fig. 6).

Integration of the ^{1}H NMR signals provides the stoichiometry of the host-guest complex, and in each case, one guest per host dimer is clearly indicated (Table 1). The widely separated signals for free and bound guests in the NMR spectra indicate that exchange of guests in and out of the cavity is slow on the NMR time scale.

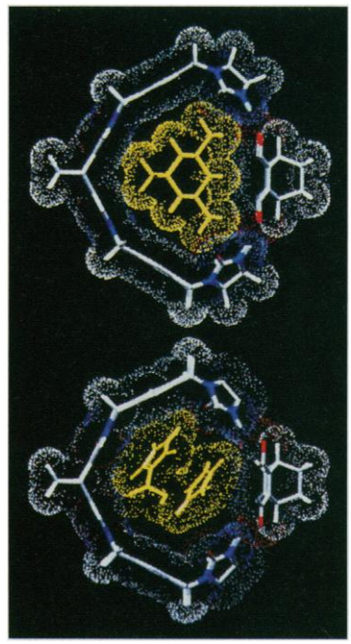

Fig. 6. Host-guest complexes. Energy-minimized models with cutaway views showing the van der Waals radii of the complex with tetramethyladamantane (top) and 1-ferrocenecarboxylic acid (bottom) encapsulated in dimer **1b**. The R groups have been omitted and the guests colored yellow for clarity.

The inclusion studies indicate that the functionality of the guest can be most important in organizing the assembly. The addition of only 1 equivalent of the functionalized adamantane derivatives to the solution of **1b** produced the sharp spectrum indicative of a well-ordered dimeric assembly, whereas even 10 equivalents of 1,3,5,7-tetramethyladamantane was insufficient to produce such order. Similarly, the proportion of encapsulated-to-free guest was much greater for the functionalized adamantanes (*8*), a result consistent with larger contributions of electrostatic versus van der Waals interactions (*9*).

The analysis of quantitative data obtained from the ^{1}H NMR spectra can be used to calculate equilibrium association constants for various guests. These values are here denoted as apparent association constants, K_a(app), because of the simplification of the several dynamic processes present into one process in by Eq. 1 (*10*).

$$\mathbf{1b}_{(\text{aggregate})} + \text{guest} \rightleftarrows \mathbf{1b} \cdot \text{guest} \cdot \mathbf{1b} \quad (1)$$

$$K_a(\text{app}) = \frac{[\mathbf{1b} \cdot \text{guest} \cdot \mathbf{1b}]}{[\mathbf{1b}_{(\text{aggregate})}][\text{guest}]}$$

The apparent association constants listed in Table 1 allow comparison of the relative affinities of the dimeric assembly for these guests.

In summary, the behavior and functions of molecule **1** can, to some extent, be controlled, either by solvation or encapsulation of guests. The considerations of host-guest complementarity and the sizable cavity of the dimeric capsule suggest that catalysis of reactions that feature transition states of the appropriate size, shape, and functionality may be possible within the assembly.

REFERENCES AND NOTES

1. J. Israelachvili, *Intermolecular and Surface Forces* (Academic Press, London, ed. 2, 1992); F. Diederich, *Angew. Chem.* **100**, 372 (1988).
2. For a sampling of three-dimensional supramolecular aggregates, see C. Seto and G. M. Whitesides, *J. Am. Chem. Soc.* **113**, 712 (1991); M. Simard, D. Su, J. D. Wuest, *ibid.*, p. 4696; P. Baxter, J.-M. Lehn, A. DeCian, J. Fisher, *Angew. Chem. Int. Ed. Engl.* **32**, 69 (1993); R. P. Bonar-Law and J. K. M. Sanders, *Tetrahedron Lett.* **34**, 1677 (1993); M. R. Ghadiri, J. R. Granja, R. A. Milligan, D. E. McRee, N. Khazanovich, *Nature* **366**, 324 (1993); J. Yang, E. Fan, S. J. Geib, A. D. Hamilton, *J. Am. Chem. Soc.* **115**, 5314 (1993); M. R. Ghadiri, K. Kobayashi, J. R. Granja, R. K. Chadha, D. E. McRee, *Angew. Chem. Int. Ed. Engl.* **34**, 93 (1995); J. P. Mattias, C. T. Seto, E. E. Simanek, G. M. Whitesides, *J. Am. Chem. Soc.* **116**, 1725 (1994); J. P. Mathias, E. E. Simanek, J. A. Zerkowski, C. T. Seto, G. M. Whitesides, *ibid.*, p. 4316; J. P. Mathias, E. E. Simanek, G. M. Whitesides, *ibid.*, p. 4326.
3. N. Branda, R. Wyler, J. Rebek Jr., *Science* **263**, 1267 (1994); R. Wyler, J. de Mendoza, J. Rebek Jr., *Angew. Chem. Int. Ed. Engl.* **32**, 1699 (1993); D. J.

Cram, R. Jaeger, K. Deshayes, *J. Am. Chem. Soc.* **115**, 10111 (1993); D. J. Cram, *Nature* **356**, 29 (1992); M. Fujita, N. Satoshi, K. Ogura, *J. Am. Chem. Soc.* **117**, 1649 (1995).
4. The assembly was modeled on a Silicon Graphics Personal Iris with Macromodel V3.5X, MM2 force field with the GB/SA model [F. Mohamadi *et al.*, *J. Comput. Chem.* **11**, 440 (1990)].
5. For similar reactions of *tert*-butyl hydrazodiformate, see L. A. Carpino, *J. Am. Chem. Soc.* **85**, 2144 (1963).
6. The synthesis follows that of a related tetramethyl ester [R. Beerli and J. Rebek Jr., *Tetrahedron Lett.* **36**, 1813 (1995)].
7. Introduction of the 1,3-adamantanedicarboxylic acid to the NMR tube followed by vigorous shaking for 10 s is all that is necessary to cause dissolution.
8. In the cases of the 1-adamantaneamine and 1-adamantanecarboxylic acid (Fig. 5B), the proton resonances of nonencapsulated guests are discernable in the region between 1 and 2 ppm and can be estimated to be about equal in intensity to the resonances of the included guest. For 1,3,5,7-tetramethyladamantane (Fig. 5E), the proton resonances of the nonencapsulated guest are the very large peaks whose bases are visible at 0.8 ppm; at full scale, these resonances are about 60 times as intense as the resonances of the included guest. This guest can be displaced by the addition of 20 equivalents of benzene for each equivalent of 1,3,5,7-tetramethyladamantane, indicating that benzene, by comparison, is a much less favored guest.
9. H. Dugas, *Bioorganic Chemistry* (Springer-Verlag, New York, ed. 2, 1989), pp. 20–21.
10. The value for the complex term [**1b** · guest · **1b**] was measured from the NMR spectra by using an internal standard, and the [$\mathbf{1b}_{(aggregate)}$] and [guest] values were calculated by subtracting the complex amount from the total amounts. Several assumptions were made: (i) the amount of dimer (unfilled or filled with solvent) present before addition of the guest is negligible, (ii) after addition of the guest, all the host material not assembled into the complex is in the aggregate state, and (iii) the association of the guest with itself is negligible.
11. R.S.M. thanks NIH for a fellowship, and we thank NIH for support of this research.

2 June 1995; accepted 22 August 1995

Yeast Checkpoint Genes in DNA Damage Processing: Implications for Repair and Arrest

David Lydall and Ted Weinert

Yeast checkpoint control genes were found to affect processing of DNA damage as well as cell cycle arrest. An assay that measures DNA damage processing in vivo showed that the checkpoint genes *RAD17*, *RAD24*, and *MEC3* activated an exonuclease that degrades DNA. The degradation is probably a direct consequence of checkpoint protein function, because *RAD17* encodes a putative 3′-5′ DNA exonuclease. Another checkpoint gene, *RAD9*, had a different role: It inhibited the degradation by *RAD17*, *RAD24*, and *MEC3*. A model of how processing of DNA damage may be linked to both DNA repair and cell cycle arrest is proposed.

Checkpoint controls recognize DNA damage and halt cell division until DNA repair is complete. They are thought to play an important role in tumor prevention, because human checkpoint genes, such as *p53* and *ATM*, are often compromised in tumor cells (*1*). How eukaryotic checkpoint controls work to sense DNA damage and to signal arrest is unclear. Studies in yeasts have identified genes that are essential for arrest in G_2 after DNA damage, at the G_2 checkpoint. Here we examine the role of the G_2 checkpoint genes *RAD9*, *RAD17*, *RAD24*, and *MEC3* (*2–5*) in yeast. Other genes, *MEC1*, *RAD53*, and *POLε*, are also required for checkpoint control at the S-phase checkpoint when DNA replication is blocked (*5–7*).

Checkpoint proteins could be involved in a signal transduction pathway linking DNA damage to cell cycle arrest. However, several observations suggested to us that the *RAD9*, *RAD17*, *RAD24*, and *MEC3* genes are not solely, if at all, involved in signal transduction. We found that these four checkpoint control genes can be divided into two groups based on phenotypes that suggest possible roles in DNA repair. These groups are the *RAD24* group (*RAD17*, *MEC3*, and *RAD24*) and the *RAD9* group (consisting only of the *RAD9* gene) (Table 1). We found, for example, that *rad9 rad24* double mutants are more sensitive to the DNA damage caused by ultraviolet (UV) radiation and methyl methane sulfonate (MMS) than are the corresponding single mutants (Fig. 1). Our analysis of the results summarized in Table 1 led us to test whether the *RAD9* and *RAD24* group genes

Department of Molecular and Cellular Biology, University of Arizona, Tucson AZ 85721, USA.

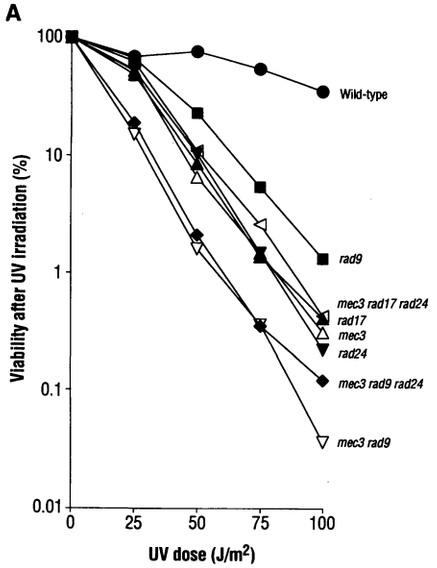

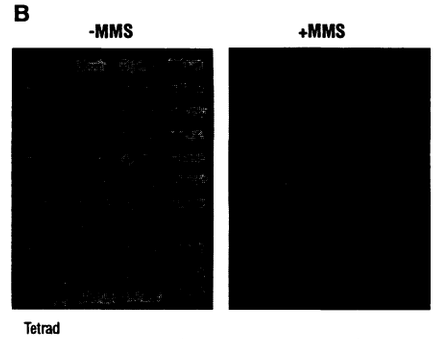

Tetrad number	a	b	c	d
1	9, 17	9	3, 17, 24	3, 24
2	3, 9	–	WT	3, 9, 17, 24
3	3, 17, 24	9	3, 9, 24	17
4	24	WT	3, 9, 17	3, 9, 17, 24
5	24	9, 17, 24	3, 17	3, 9
6	3, 9, 24	WT	9, 17, 24	3, 17
7	17, 24	3, 9	3, 17	9, 24
8	–	9, 17, 24	9, 24	–
9	3, 9, 24	9, 17	3, 24	17
10	3	3, 17, 24	9, 17	9, 24
11	3, 9, 24	3	9, 17, 24	17

Fig 1. Assignment of *rad9* mutants to a different epistasis group than *rad17*, *rad24*, and *mec3* mutants. (**A**) Sensitivity of checkpoint mutant strains to UV irradiation. A series of A364a strains in which combinations of the *RAD9*, *RAD17*, *RAD24*, and *MEC3* genes had been deleted were tested for their sensitivity to UV irradiation. All the survival curves shown were obtained on the same day. There was slight day-to-day variation in cell viability, but whenever a *rad9* mutation was combined with any other checkpoint mutation the cells were more sensitive to UV irradiation. Experiments in the W303 background produced a similar pattern (*16*). (**B**) Sensitivity of checkpoint mutant strains to the alkylating agent MMS. Strain DLY 217 (A364a background, *Mat**a** rad9::HIS3 rad17::LEU2 rad24::TRP1 mec3::URA3*) was crossed to strain DLY221 (A364a background, *Matα his3 leu2 trp1 ura3*). The diploid was sporulated, and all possible combinations of mutations were found in the haploid progeny. Strains were replica-plated to YEPD-rich plates (containing yeast extract, peptone, and dextrose) with (+) or without (−) 0.01% MMS. In addition, the progeny from each tetrad (labeled a, b, c, or d in table) were replica-plated to −URA, −HIS, −LEU, and −TRP plates to determine which checkpoint mutations were present. Abbreviations in table are as follows: 3, *mec3::URA3*; 9, *rad9::HIS3*; 17, *rad17::LEU2*; 24, *rad24::TRP1*; and WT, wild type. A dash indicates that this particular spore did not grow. Three levels of growth were observed in the presence of MMS: Wild-type cells were MMS-resistant, *rad9* or *rad24* group mutants were sensitive, and *rad9 rad24* group double mutants were supersensitive. Consistent results were found in the W303 genetic background (*16*).